Environmental Pollution 233 (2018) 782–796

Contents lists available at ScienceDirect

Environmental Pollution

journal homepage: www.elsevier.com/locate/envpol

How tall buildings affect turbulent air flows and dispersion of pollution within a neighbourhood☆

Elsa Aristodemou [a, b, *], Luz Maria Boganegra [a], Laetitia Mottet [b], Dimitrios Pavlidis [b], Achilleas Constantinou [a, c], Christopher Pain [b], Alan Robins [d], Helen ApSimon [e]

[a] School of Engineering, London South Bank University, London, UK
[b] Department of Earth Sciences, Imperial College London, London, UK
[c] Department of Chemical Engineering, University College London, London, UK
[d] Department of Mechanical Engineering Sciences, University of Surrey, Surrey, UK
[e] Department of Environmental Policy, Imperial College London, UK

ARTICLE INFO

Article history:
Received 13 May 2017
Received in revised form
21 September 2017
Accepted 11 October 2017

Keywords:
Air pollution
Computational modelling
Large eddy simulations
Urban environment
Wind tunnel experiments

ABSTRACT

The city of London, UK, has seen in recent years an increase in the number of high-rise/multi-storey buildings ("skyscrapers") with roof heights reaching 150 m and more, with the Shard being a prime example with a height of ~310 m. This changing cityscape together with recent plans of local authorities of introducing Combined Heat and Power Plant (CHP) led to a detailed study in which CFD and wind tunnel studies were carried out to assess the effect of such high-rise buildings on the dispersion of air pollution in their vicinity. A new, open-source simulator, FLUIDITY, which incorporates the Large Eddy Simulation (LES) method, was implemented; the simulated results were subsequently validated against experimental measurements from the EnFlo wind tunnel. The novelty of the LES methodology within FLUIDITY is based on the combination of an adaptive, unstructured, mesh with an eddy-viscosity tensor (for the sub-grid scales) that is anisotropic. The simulated normalised mean concentrations results were compared to the corresponding wind tunnel measurements, showing for most detector locations good correlations, with differences ranging from 3% to 37%. The validation procedure was followed by the simulation of two further hypothetical scenarios, in which the heights of buildings surrounding the source building were increased. The results showed clearly how the high-rise buildings affected the surrounding air flows and dispersion patterns, with the generation of "dead-zones" and high-concentration "hotspots" in areas where these did not previously exist. The work clearly showed that complex CFD modelling can provide useful information to urban planners when changes to cityscapes are considered, so that design options can be tested against environmental quality criteria.

1. Introduction

Optimising the building infrastructure and minimising the effect of emissions of air pollutants within the urban environment requires reliable and accurate predictions of both the turbulent air flows and concentration predictions at high temporal and spatial resolutions. This implies solving the time-dependent, three-dimensional, non-linear Navier-Stokes equations together with the advection-diffusion and chemical reaction equations for the concentration of pollutants, as well as the turbulent diffusion equations on *highly resolved* spatial computational meshes at reasonable computational speeds. In addition, representing and capturing accurately the turbulence and its statistics within the computational domain, thus leading to an enhanced understanding of the physical mixing processes and exchange rates (for both momentum and pollution concentrations) at pedestrian levels and at levels well above the roof tops, is also crucial (Zhou and Hanna, 2007; Solazzo and Britter, 2007). These two aspects: (a) numerical solutions at high temporal and spatial resolutions and (b) accurate as representation of the air flow and turbulence have been the most challenging problems for air quality studies over the last 40 years, leading to the development of both new computational

☆ This paper has been recommended for acceptance by Charles Wong.
* Corresponding author. School of Engineering, London South Bank University, London, SW1 0AA, UK.
E-mail addresses: aristode@lsbu.ac.uk, e.aristodemou@imperial.ac.uk (E. Aristodemou).

https://doi.org/10.1016/j.envpol.2017.10.041

methodologies for the representation of turbulence, as well as the implementation of these methodologies on adaptive computational meshes. It is the aim of the research presented in this paper to introduce and show detailed results from a new numerical Large Eddy Simulation (LES) approach within the FLUIDITY software (http://fluidityproject.github.io/) that addresses both challenges. The novelty of the work is based on: (i) the implementation and validation of an innovative LES approach that combines an anisotropic eddy viscosity tensor for the subgrid modelling with adaptive meshes; this allows accurate representation of the turbulence at high spatial resolutions and enables the detailed capture of the turbulent eddies formed within the domain at pedestrian-level scales; (ii) the utilisation of new wind tunnel data for a specific 7-builing configuration representing a real set of buildings in central London; and (iii) the implementation of the software and qualitative assessment of the effect of tall buildings on atmospheric pollution dispersion.

Adaptive meshes began to appear in the early 1990s with the work of Benson and McRae (1991) on structured grids, followed by Odman et al. (1997) utilising an embedded Cartesian grid approach, and Tomlin et al. (1997) with adaptivity on unstructured grids for 2D problems. The adaptive algorithm of Benson and McRae (1991), DSAGA, has since been implemented by several authors in urban pollution problems, with Srivastava et al. (2000) using it in air quality models, capturing the changes in concentration distributions and their gradients due to advection as well as chemical reactions and dispersion of a pollutant puff (Srivastava et al., 2001a,b).

Tackling the second challenge of representing the turbulence within atmospheric flows, traditionally, the k-epsilon turbulence models (Reynolds Averaged Navier Stokes methodology (RANS)) have been implemented for air pollution studies. However, Coirier et al. (2005) and Di Sabatino et al. (2008) emphasised in their studies that underpredicting the turbulent kinetic energy can lead to erroneous concentration predictions, and hence concluded that representing the turbulence accurately within a model is just as important as grid refinement, if not more so. Understandably, the upward/vertical movement of pollution from the lower heights of the street canyons to higher up (through the overlying shear layer and into the boundary layer above) is of major interest in air pollution studies. In the past, for the two-dimensional canyons, this transfer has been assumed to be directly related to the external flow/velocity (http://envs.au.dk/en/knowledge/air/models/ospm/). However, Baik and Kim (2002) showed that not only the vertical mean velocities are important, but also the vertical turbulent velocities, resulting in pollutants escaping through these turbulent processes, whilst the overall effect of the mean flow can lead to the re-entrance of some of the escaped pollutants back into the street. They also confirmed their findings by varying the inlet velocities and turbulence intensities, as well as varying canyon aspect ratios. Caton et al. (2003) carried out a similar study investigating both analytically and experimentally the dispersion mechanisms in two-dimensional canyons. They showed how the turbulent inflow properties influence the vertical transfer of pollutants and are just as important as the external mean flow. Kim and Baik (2003) also discuss how the inlet turbulent intensity conditions affect the dispersion of pollution downstream. In their study, the authors describe how the pollutants are transported upwards or downwards, depending on the strength of the eddy diffusion and advection at different heights, and the influence of the main and secondary canyon vortices. They confirmed that by increasing the inflow turbulent intensities, pollution concentrations within the street decrease, whilst the upward movement of pollution is enhanced. The importance of the inlet turbulent conditions for the accurate prediction of mean concentrations is also highlighted in the study of Milliez and Carissimo (2007). In their study, the authors discuss how the k-epsilon turbulent model parameters affect the predicted concentrations and their associated statistics. Sensitivity studies on the fluctuations in the source emission rate showed little effect. Similarly, the RANS studies carried out by Coirier et al. (2005) and later by Di Sabatino et al. (2008) emphasised the importance of representing as accurately as possible the turbulence characteristics, as underpredictions could lead to erroneous concentration predictions. The authors also make the interesting comment that should the need for short-term responses arise for risk assessment purposes, it would mean that peak concentrations must be evaluated, which can be only achieved more appropriately using methodologies such as the large eddy simulations (LES).

The LES method is currently one of the most favoured and computationally powerful approaches for simulating complex turbulent flows as it enables unsteady flows to be captured at high temporal and spatial resolutions. As such, it provides additional information of both the fine flow structures developed as well as of the turbulence statistics, leading to a greater understanding of the physical processes taking places within street canyons. Its strength lies in its computational efficiency, as it simulates and resolves the larger-scale eddies/turbulent structures explicitly whilst modelling the unresolved/small-scale ones; this leads to faster computations compared to DNS simulations, and more accurate representation of the turbulent fields compared to the RANS approaches. The LES method for atmospheric flows was first proposed by Smagorinsky (1963) and since then it has been facilitated by the rapid growth in computing power, thus enabling it to enter mainstream engineering. Piomelli (1999) summarises the achivements and challenges of the LES method up to the end of the 20th century, whilst Zhiyin (2015) presents a detailed review of the method, outlining its progress since its initial appearance in the 1960s and how it has entered mainstream engineering in the last two decades. In addition, the author describes the challenges, past and present for the LES method, with regards to the range of turbulent length scales it needs to represent during transient simulations, as well as the theoretical developments that have been carried out over the years in order to represent turbulent inlet conditions, and subgrid scale models. Within the LES approach, the smaller eddies have traditionally been modelled with the Smagorisnky eddy viscosity model (Smagorinsky, 1963). In the initial version of the model, the Smagorisnky coefficient required for the determination of the eddy viscosity was kept constant. However, it was later recognised that this assumption may lead to over-dissipation of the sub-grid scale turbulent kinetic energy, and thus efforts since the 1990s have taken place leading to a variety of subgrid scale models based on: (a) an eddy viscosity representation only; (b) the similarity models where filtering methods are used to deduce the subgrid scale model from the resolved stress tensor values; and (c) the mixed models, which integrate the eddy-viscosity approach within the similarity models (Sagaut, 1998).

Apart from the numerous choices of sub-grid scales models within the LES approach, adaptive grids were also implemented, with one of the earliest implementations being the work of Wissink et al. (2005) with a Cartesian Adaptive Mesh Refinement (AMR) capability. This was followed by the work of Ghorai et al. (2000) where we also see an implementation of a three-dimensional, time-dependent gridding technique for dispersion problems in neutral, stable, and unstable atmospheric boundary layers. Walton and Cheng (2002) implemented LES using a structured grid, for street canyons in Hong-Kong, with an aspect ratio (Height/width) of 1.2. A dynamic LES subgrid-scale model was implemented, together with periodic boundary conditions. Based on the comparisons between simulations and wind-tunnel data, the authors

concluded that the most important physical process in removing the pollutants from the street canyons is the motion of the larger turbulent eddies rather than the steady diffusion resulting from smaller scale turbulence. They also found that the LES simulations predicted a considerably higher turbulent kinetic energy within the core of the vortex, and hence enhanced mixing and dispersion compared to RANS results. An interesting and informative study of *reactive* pollutants (NO, NO_2 and O_3) using the LES approach is described by Baker et al. (2004) which looks at the spatial variation of these contaminants in an idealised street canyon configuration. Their results showed that concentrations of NO and NO_2 were higher in the downwind side as opposed to the side facing the wind, thus being consistent with the outcome of the studies by Baik and Kim (2002) and Xie et al. (2003). In these studies, the traffic emissions are believed to be entrained and dispersed by the primary flow vortex. The authors also found that a strong shear layer would also be responsible for the "trapping" of pollution. At the places/locations where the shear layer destabilises, thus becoming more turbulent, there is a stronger vertical air exchange between the canyon and the layers higher up, thus resulting in lower concentration gradients, and a "smoother" vertical concentration profile. The work of Porte-Agel (2004) discusses the development of the varying versions of the dynamic Smagorinky LES models, and comparisons with experimental data within the atmospheric boundary layer. More recent studies discuss CFD applications for urban micro-climate, incorporating heat island effects, chemical reactions (Střižík et al., 2014), as well as the effect of building layouts and presence of upstream buildings to the downstream ones. Toparlar et al. (2015) implements unsteady RANS simulations to study the heat island effects through heat transfer by conduction, convection and radiation in a case study area in Rotterdam (Netherlands), whilst Cui et al. (2016) discuss the effect of the presence of an upstream building to indoor pollution levels in a downstream multi-story building. Gromke and Blocken (2015) study the effect of green-infrastructure (trees) on naturally ventilated areas and subsequent air quality through a series of RANS-based CFD simulations which included the aerodynamics effects of not only the buildings, but also of trees. The effect of green infrastructure/urban vegetation is of great interest to both researchers and urban planners, with a recent review by Janhall (2015) which identifies which types of vegetation would be most appropriate and at what locations they should be placed within the urban environment for enhancing the deposition and dispersion of specifically particulate matter. A recent interesting modelling study (using the realisable *k-epsilon* model) looking at the dispersion of dust particles (due to a dust storm) within a residential area has been carried out by Luo et al. (2016), whilst a computational study looking at the effects of building layouts with tree arrangements on thermal comfort at pedestrian level has been carried out by Hong and Lin (2015); their modelling simulations considered an air flow model together with a vegetation model that incorporated the amount of heat absorbed by leaves, as well as the amount of heat convection, and the process of transpiration by the leaves. Their study emphasises the importance of using numerical studies/modelling for optimising building design layouts together with green infrastructure for optimal thermal comfort within the urban environment, as well as the reduction of pollution levels. The effect of outdoor air pollution on indoor levels of pollution, for either naturally or mechanically ventilated/aerated buildings is a topic that has also been gaining momentum the past few years, highlighting the importance of improving outdoor air quality. One such study has been carried out recently by Tong et al. (2016), which implemented CFD simulation for assessing the effect of various building parameters/design and ventilation strategies for improving indoor air quality, particularly with respect to aerosols/particulate matter. Studying the effect of tall buildings on the flow characteristics has also been of great interest to urban planners, with studies such as the one carried out by Heist et al. (2009), which looked at the effect of a single tall tower on the air flows within in a residential area in New York. More recent studies such as the one by Yu et al. (2017), which look at the effect of high-rise buildings on air pollution dispersion for different wind directions illustrate the importance of carrying out complex CFD simulations for studying the effect of the changing cityscapes on air pollution.

The many CFD applications and attempts for modelling dispersion of pollutants within the urban environment emphasise the continuous endeavours to address both the need of realistic representation of cityscapes - through enhanced spatial resolution - as well as accurate predictions for both flow and concentrations. It is now widely recognised that adaptive grids/meshes are necessary for enhanced accuracy of both flow and pollution concentration predictions through accurate capturing of the flow turbulence and its effect on the dispersion of the pollutants (at the short timescales that affect human health), although less-computationally intensive models have also been developed and implemented recently in order to address the emergency-response scenarios (Zhang et al., 2016). The implementation of mesh-adaptivity for atmospheric boundary layer pollution/air quality studies is relatively new. The first LES methodology to be developed and implemented on unstructured and adaptive meshes was based on the work of Bentham (2004), whilst Constantinescu et al. (2008) showed how higher resolution meshes are necessary both near the pollution emission points and at distances further upwind. Aristodemou et al. (2009, 2016) implemented the adaptive LES approach developed by Bentham (2004) and showed its strength by comparing the simulated results with wind tunnel measurements. Following on from this work, the two key objectives of the current work are: (a) to assess further the capability of the LES methodology developed by Bentham (2004) by demonstrating how the two main challenges in air pollution studies, namely the required high spatial and temporal resolutions and accurate representation of turbulence, are both addressed; and (b) was to implement the LES approach in order to demonstrate in detail the effect of building heights on air pollution dispersion within cities.

2. Methodology

The LES method has gained considerable popularity over the last decade, as computing power has increased dramatically and also the method itself enables the utilisation of adaptive meshes at reduced computational costs. Highly-resolved meshes are an essential requirement for enhanced accuracy for complex computational predictions that involve turbulent flows (Pope, 2000). For enhanced accuracy in the atmospheric boundary layer predictions (both for air flows and pollution concentrations), the LES approach provides a realistic and useful compromise between the traditional RANS methodology and the highly expensive (computationally) Direct Numerical Simulation (DNS) approach (Coceal et al., 2007). The LES approach utilised in this research is characterised by the advancement of a unique adaptive-mesh (unstructured) capability combined with an anisotropic subgrid scale eddy viscosity model. The equations for flow and concentration prediction are solved using high/second-order schemes in space and time that are specifically developed for unstructured grids (Pain et al., 2001). The adaptivity approach within FLUIDITY produces anisotropic tetrahedral elements and allows a large number of finer elements to be placed in the regions of the domain where the physical processes are important, whilst a coarser mesh is used in the regions of less interest; elements are produced or deleted based on a metric (as chosen by the user) and applied to any of the variables within the

domain (velocity, tracer concentration, pressure, temperature); different metrics can be applied to each variable (Fluidity manual, 2016). FLUIDITY can also be run in parallel (using MPI) on a number of processors (Gorman et al., 2003), thus further optimising the computational efficiency and enabling detailed/highly-resolved meshes to be produced at reasonable computational times/costs. This is very important for complex turbulent flow problems such as those encountered in the atmospheric urban environment.

Initial validations of the LES methodology applied in this research have already been reported (Bentham, 2004; Aristodemou et al., 2009) as comparisons of velocity field predictions with data from the University of Surrey EnFlo wind tunnel (https://www.surrey.ac.uk/mes/research/aef/enflo/). One focus of EnFlo research is the study of pollution dispersion in the atmospheric boundary layer (Carpentieri and Robins, 2015; Belcher et al., 2015) and further data for validation of the FLUIDITY LES approach have been provided (Robins, 2016; personal communication), thus allowing the continuation and extension of the initial work presented in Aristodemou et al. (2016). A detailed study of the effect of building heights on local-scale tracer dispersion was completed based on this validation exercise.

2.1. The mesh-adaptive large eddy simulation approach

The LES equations implemented in this work are based on the theoretical work developed by Bentham (2004) and Pain et al. (2001) as found within the FLUIDITY software (http://fluidityproject.github.io/), in which and in Pavlidis (2010). A key aspect of the LES method is the anisotropic eddy viscosity subsgrid scale model. The basic LES equations describing turbulent flows are based on the filtered (three dimensional) incompressible Navier Stokes equations (continuity of mass and momentum equations) are as follows:

Mass Continuity

$$\frac{\partial \tilde{u}_i}{\partial x_i} = 0 \quad \text{or} \quad \nabla \cdot \tilde{u} = 0 \tag{1}$$

Momentum

$$\frac{D\tilde{u}}{Dt} = -\frac{1}{\rho}\nabla \tilde{P} + \nabla \cdot \left[\left(\nu + \nu^{eddy} \right) \nabla \tilde{u} \right] \tag{2}$$

where $\tilde{u}$, and $\tilde{P}$ represent (respectively) the resolved/filtered velocity and pressure fields in the cartesian system, whilst ρ is the density of the incompressible fluid; the kinematic viscosity of the fluid (air) is denoted by ν whilst υ^{eddy} is the anisotropic eddy viscosity, which the unresolved/subgrid scale stress tensor τ depends on.

A novel component in the implementation of the standard LES equations within FLUIDITY is the anisotropic eddy viscosity tensor, $\upsilon^{eddy} = (C_s \Delta)^2 \left| \tilde{S} \right|$ linked to the adaptive mesh, where C_s is the Smagorisnki constant (C_s takes the value of 0.11); the filter length is denoted by Δ and is dependent on the local element size as shown further below; $\left| \tilde{S} \right|$ is the characteristic filtered rate of strain, dependent on $\tilde{S}_{ij}$ which is the local filtered strain rate tensor; they are both determined through the following expressions:

$$\tilde{S}_{ij} = \frac{1}{2}\left(\frac{\partial \tilde{u}_i}{\partial x_j} + \frac{\partial \tilde{u}_j}{\partial x_i} \right) \quad \text{whilst} \quad \left| \tilde{S} \right| = \left(2\tilde{S}_{ij}\tilde{S}_{ij} \right)^{1/2} \tag{3}$$

One of the novelties of the implemented LES code lies in the fact that local filter length Δ depends on the local element size $\left(h_\zeta, h_\eta, h_\xi \right)$ according to the following relationship $\Delta = 2 \times \left(h_\zeta, h_\eta, h_\xi \right)$ (local element co-ordinate system). Rotational transformations V^T and V are used to transform from the one co-ordinate system (local) to another (global), leading to the inverse of a mesh-adaptivity metric M given by:

$$M^{-1} = V^T \begin{bmatrix} h_\zeta^2 & 0 & 0 \\ 0 & h_\eta^2 & 0 \\ 0 & 0 & h_\xi^2 \end{bmatrix} V \tag{4}$$

Thus, the anisotropic eddy viscosity tensor is determined through the expression:

$$\begin{aligned} \upsilon^{eddy} &= C_s^2 \left| \tilde{S} \right| V^T \begin{bmatrix} \Delta_\zeta^2 & 0 & 0 \\ 0 & \Delta_\eta^2 & 0 \\ 0 & 0 & \Delta_\xi^2 \end{bmatrix} V \\ &= 4C_s^2 \underbrace{\left| \tilde{S} \right| V^T \begin{bmatrix} h_\zeta^2 & 0 & 0 \\ 0 & h_\eta^2 & 0 \\ 0 & 0 & h_\xi^2 \end{bmatrix} V}_{M^{-1}} \end{aligned} \tag{5}$$

The spatial gradients of the subgrid stress tensor τ are determined through the expression:

$$\nabla \cdot \tau = \nabla \cdot \left[\left(\upsilon^{eddy} \right) \nabla \tilde{u} \right] \tag{6}$$

As an example of the variation of the anisotropic eddy viscosity with the adaptive grid, the υ_{xx}^{eddy} (xx-diagonal) component of the eddy viscosity tensor, together with the corresponding velocity field (in the x-y plane) are shown in Fig. 2.

Further details of the method as implemented in the FLUIDITY software can be found in Bentham (2004) and Pavlidis (2010).

2.2. The computational domain

The computational domain was based on the wind tunnel configuration representing the seven buildings as shown in Fig. 1; the building dimensions used are as in the wind tunnel (Table 1). The wind tunnel configuration represented a set of realistic buildings in an area in central London (as shown in the supplementary document), with scaling of 1:200. For the LES simulations, additional scenarios were set-up by hypothetically increasing the building heights as shown in Table 1. The passive tracer source was placed at the top of building A, at coordinates (−0.01875 m, 0.01875, 0.1508 m), representing a potential CHP emission source. The dimensions of the computational domain were based on the building dimensions within the wind tunnel, and covered a volume of 4.0 m by 2.0 m by 2.0 m, allowing a relatively long-development section for the formation of a deep boundary layer in the LES simulations. Simulations were carried out with: (i) a constant velocity inlet condition, and (ii) two slightly different turbulent velocity inlets so that an assessment of the effect of the inlet flow conditions could be made. The downstream boundary (outlet) was left as pressure boundary (no-stress condition), whilst the remaining boundary conditions consisted of: (i) the “no slip” condition for the solid walls of buildings and “floor” of domain, and (ii) the “no shear” condition for the free surfaces (sides and the top of the domain).

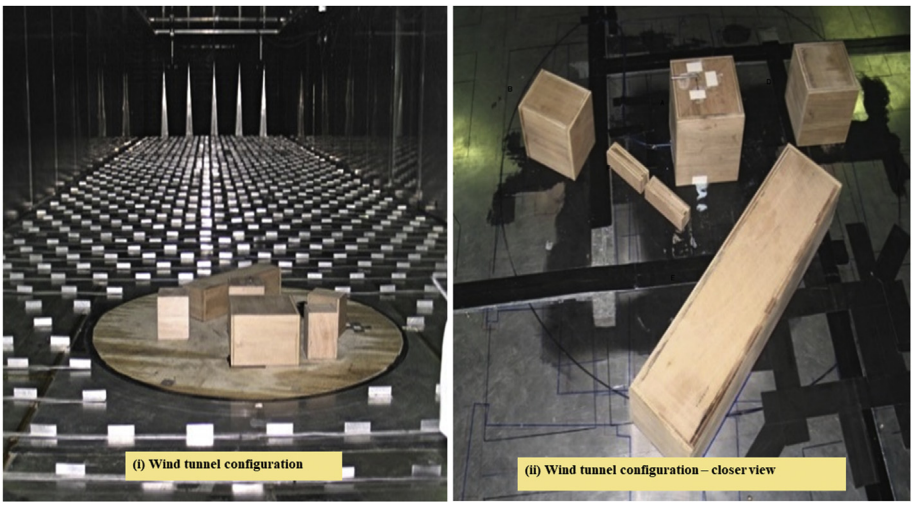

Fig. 1. The model installed in the wind tunnel (Robins, 2016; personal communication).

2.3. Mesh adaptivity

One of the key and innovative aspects of the FLUIDITY software is its mesh-adaptivity capability on unstructured meshes making it a unique tool that enhances and provides detailed and accurate information at high resolutions within the computational domain. The process of adaptive re-meshing consists of three parts: (i) deciding what mesh is desired; (ii) generating this mesh; and (iii) transferring information to the latest mesh from the older one, based on a metric as chosen by the user (Fluidity manual, 2016). The process allows several actions to be taken such as: (i) addition and reduction of the number of nodes and elements, leading subsequently to refining or coarsening of the mesh; and (ii) smoothing of the mesh by moving nodes whilst keeping the overall number of elements and nodes the same. Adaptivity within FLUIDITY is based on *a-posteriori error* estimates, which aim at achieving certain targets for error, and incorporate what are known as: (i) *h-adaptivity* (associated with mesh connectivity); (ii) *p-adaptivity* – linked with polynomial orders; and (iii) the *r-adaptivity* (associated with relocation of element vertices) (Fluidity Manual, 2016). A combination of these can also be set e.g. *hr-adaptivity*, which was implemented in this study. Adaptivity options can be field-specific (i.e. different computed fields can be configured with their own specific adaptivity options) but also non-field specific options can be set.

For the simulations in this study, field-specific adaptivity options (Interpolation Error bound value, as well as the type of interpolation) were assigned to the velocity (vector) field and the tracer (scalar) field. For both fields, the type of interpolation was set to the "consistent interpolation" option. For the more general non-field adaptivity options, mesh resolution can also be controlled by specifying the maximum/minimum sizes of the elements, at different areas within the domain. In our simulations, the minimum and maximum element sizes were set to 0.003 m and 0.004 m respectively around the location of the source, on top of building A (S2(a)); hence, finer-resolution can be "forced" in specific regions within the computational domain. In addition, the user can also control as to how often the adaptivity process can take place e.g. every so many timesteps, as opposed to every time step. For this study, the mesh was adapted every 15 timesteps. Anisotropic gradation was also allowed in the simulations, as well as an adaptive time-step based on a CFL number of 0.9. The maximum number of nodes can also be set; for our simulations, this was set to 400,000 nodes, rendering approximately one million elements. Absolute and relative convergence errors were set to 10^{-12} and 10^{-7} respectively. Further details on the method of mesh-adaptivity and the metrics used can be found in Pain et al. (2001), as well as the Fluidity manual (2016). Examples of the adaptivity effect on the computational mesh are shown extensively in section 3 (Results section).

2.4. Wind tunnel experiments

The wind tunnel data, as provided by Robins (2016) (personal communication), were obtained from a set of experiments carried out in the EnFlo wind tunnel for a seven-building site configuration (Fig. 1 and Table 1), based on actual buildings/local neighbourhood in central London. However, the seven buildings were studied in isolation in the wind tunnel, not as part of a larger urban model, to simplify the overall complexity of modelling the experiments in CFD codes. The 1:200 scale wind tunnel model was installed in the tunnel in a fully developed, 1 m deep, simulated atmospheric boundary layer and dispersion experiments carried out using a reference wind velocity U_{ref} being 2.1 m/s. The simulated atmospheric boundary layer represented near-neutral atmospheric conditions and was initiated by a set of Irwin spires (vorticity-generators) at the inlet to the wind tunnel working section, with roughness elements on the floor to maintain the surface roughness condition. The boundary layer depth was 1000 mm, the surface roughness length 1.5 mm and the friction velocity $0.057U_{ref}$, with U_{ref} the air speed at the edge of the boundary layer. A passive tracer was emitted from a horizontal source above Building A (S2(a) – Building A, the Garden building) and measurements were taken for varying wind directions and model configurations. The source height was 0.1508 m, relative to a building height of 0.143 m. Mean tracer concentrations were measured using Combustion Fast Flame Ionisation Detectors (FFIDs) carried on a three-dimensional traverse system. In what follows, mean concentration data over the full model for one wind direction are used to evaluate the performance of FLUIDITY modelling.

2.5. Turbulent inlet boundary conditions

The properties of the fully developed boundary layer were measured in the wind tunnel, upstream of the building model. This included the profiles of mean speed and all the non-zero Reynolds

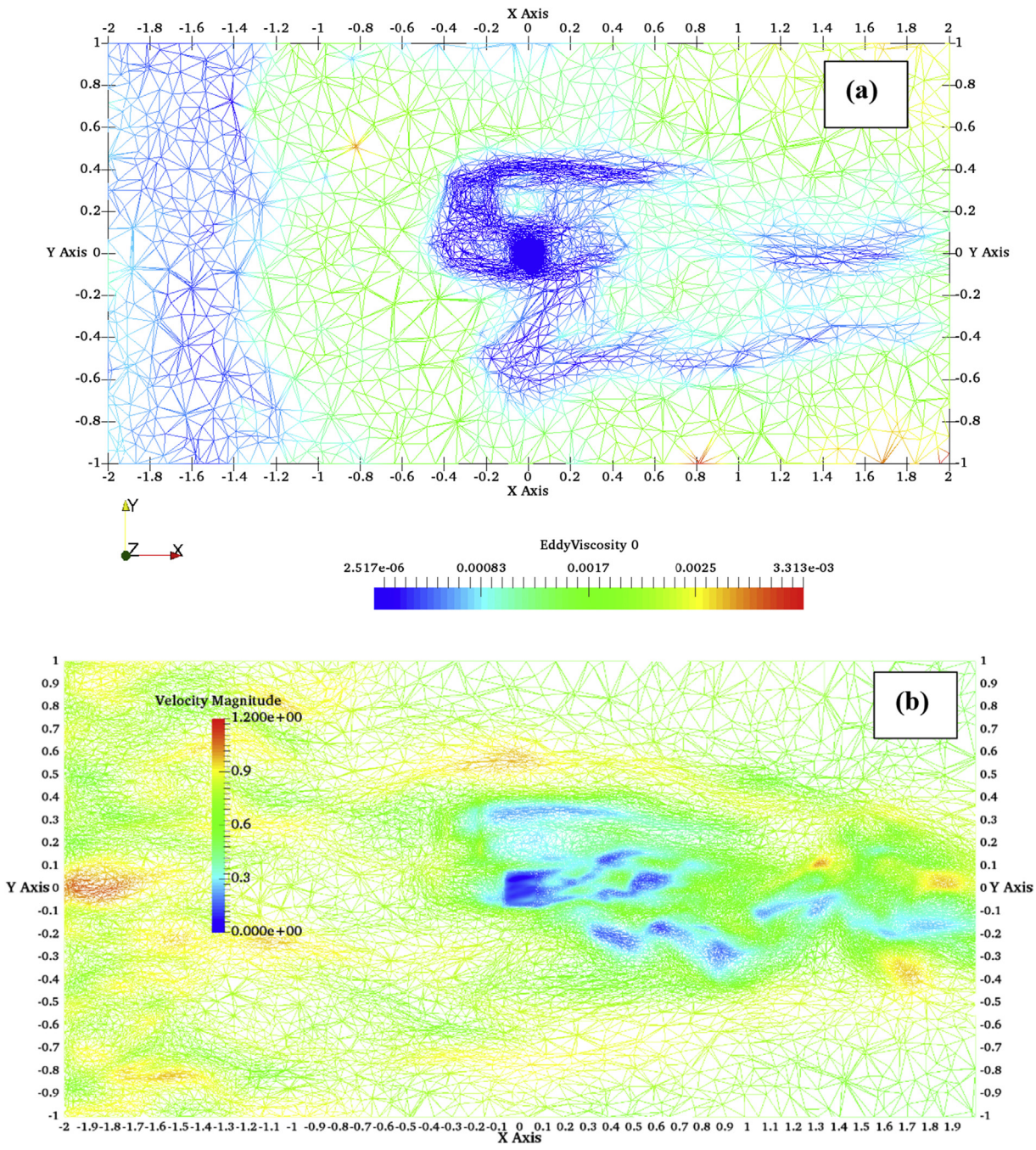

Fig. 2. **(a)** The simulated Eddy Viscosity tensor component ν_{xx}^{eddy} linked with the adaptive mesh, and utilised during the estimation of the spatial gradients of the subgrid scale tensor τ; **(b)** the corresponding resolved velocity field. *Note: Unit of distance along all axes is in metres.*

Table 1
Building heights used in the LES simulations.

Building Identification	Case 1 (wind tunnel configuration)	Case 2	Case 3
A (Garden building)	**0.1428**	**0.1428**	**0.1428**
B (Park building)	0.1238	0.4	0.4
C (Exhibition building)	0.1315	0.4	0.4
D (High street building)	0.1228	0.4	0.4
E (Melbury building)	0.0971	0.2	0.2
F (Garage building)	**0.0315**	**0.2**	**0.6**
G (Park close building)	0.1152	0.25	0.25

stresses (Supplementary document, S1). These observations were used to form inlet boundary conditions in the LES simulations, using the synthetic eddy method of Jarrin et al. (2006), as implemented in the FLUIDITY LES model by Pavlidis (2010). The synthetic eddy method is based on the superposition of coherent structures for the generation of turbulence, reproducing the required first and second order statistics, turbulence length scales and timescales for fully turbulent flows. The inlet turbulent boundary velocity $u_{bc}(x, t)$ is determined through the expression:

$$u_{bc}(x,\ t) = \overline{u}(x) + \alpha^{in} \times u'(x,\ t) \tag{7}$$

where $\overline{u}(x)$ is the mean velocity whilst $u'(x,\ t)$ represents the fluctuating component. The matrix α^{in} is a matrix whose elements depend on the specified Reynolds stresses at the inlet boundary:

$$\alpha_{ij}^{in} = \begin{pmatrix} \sqrt{R_{11}} & 0 & 0 \\ R_{21}/\alpha_{11} & \sqrt{R_{22} - \alpha_{21}^2} & 0 \\ R_{31}/\alpha_{11} & (R_{32} - \alpha_{21}\alpha_{31})/\alpha_{22} & \sqrt{R_{33} - \alpha_{31}^2 - \alpha_{32}^2} \end{pmatrix} \tag{8}$$

The calculation of the fluctuating component $u'(x,\ t)$ requires the introduction of a number of coherent structures known as turbulent spots. These turbulent spots are defined using a specific shape function $f_\sigma\ (x,\ t)$ (either Gaussian or triangular) within a bounding box; the dimensions of the bounding box are based on the actual dimensions of the boundary plane and the integral length scale. Within the current simulations the triangular shape function was used. The location and number of the turbulent spots are denoted by x_σ and n_σ respectively. The fluctuating component of the velocity is subsequently determined using the expression:

$$u' = \frac{1}{\sqrt{n_\sigma}} \sum_{j=1}^{n_\sigma} \varepsilon_j \times f_\sigma\left(x - x_{\sigma j}(t)\right) \tag{9}$$

Where ε_j is a sign vector which randomly takes the value of either $+1$ or -1. The turbulent spots are propagated through the domain based on the mean inflow velocity and the time steps, regenerating themselves at new locations as soon as they reach the downstream end of the bounding box.

This approach was implemented within the FLUIDITY software due to its compatibility with unstructured and adaptive meshes. Within the current simulations the number of turbulent spots used was set to 4000 and the required turbulent length scales and Reynolds stresses were based on the wind tunnel data.

3. Validation study

3.1. LES simulation results compared to with wind tunnel data

A Dell Precision Tower 7810 computer (dual Intel Xeon Processor) was used for the LES simulations, for a total simulation run time of ten seconds, corresponding to the same amount of real time i.e. ten seconds. The main simulated variables as functions of time were pressure. velocity and tracer concentrations. The time-variability of the concentrations is important particularly when in depth-studies of pollution exposure and subsequent effects to health are required. The normalised mean concentrations from the LES simulations – at several detectors - were determined based on the time-series results, and subsequently compared with the measured wind tunnel data (normalised mean concentrations). The LES simulations were run with *three* different velocity inlet conditions: (i) a *constant (laminar) velocity inlet*, (velocity of 1.0 m/s); this was the simplest inlet boundary condition to be considered, and it was implemented for comparison purposes; (ii) a *Turbulent-Inlet-1* representing a logarithmic inlet velocity profile similar to the measured wind tunnel profile, and a hypothetical set of Reynolds stresses lower than the wind tunnel ones; (iii) a *Turbulent-Inlet-2* representing again a logarithmic velocity profile at the inlet, but this time based on the wind tunnel measurements of both the mean flow and Reynolds stresses (supplementary document, S1). Results from the comparison study are shown in Fig. 4 along several lateral traverses within the domain (shown in the supplementary document, S2) i.e. as functions of y at fixed x and z. Overall, the x range covered was from 0.119 m to 1.224 m, the y range from −0.60 m to 0.60 m and the z range from 0.065 m to 0.30 m (note that the height of Building A was 0.143 m, with the source centre at 0.1508 m). The set of detectors to the right of building C (x = 0.203 m) at low heights (z = 0.065 m) showed greater inconsistency between simulations and measurements and this could be due to the less accurate determination of the turbulent field in those locations.

A scatter plot showing the comparison between all the LES simulations (for Case1) and wind tunnel measurements, for the 81 detectors, is shown in Fig. 3, with percentage errors ranging between 3% and 37%, although higher inconsistencies (>50%) existed in certain detector locations. Some pertinent observations follow from the comparisons:

a) The inlet conditions played a major role in the comparisons for the detectors within the building-area, with the *constant velocity inlet* scenarios resulting in the worst correlations between wind tunnel data and simulated results for detectors along lines L1, L2, L3 and L5 (S2(a)); however, when the inlet was represented with the turbulent characteristics as measured in the wind tunnel the correlations were improved considerably, for both the overall trend along traverses and the magnitude of concentrations. The best correlations between measurements and simulations (for detectors within the building area) were based on the *Turbulent-Inlet-2* simulations, indicating that the LES simulations capture the complex turbulent flow field, and hence the mean tracer concentrations.
b) Detectors well away from the building area ($x = 0.751$ m) and at heights (z = 0.3 m) well *above* the source (detectors along line L9) showed better comparisons with wind tunnel data when inlet conditions were constant.
c) Detectors away from the building area but at medium (not far from the source) heights levels (along lines L7 and L8, Fig. 4) showed similar simulation results from the three different inlet conditions – indicating that at certain locations away from the building area, the inlet conditions seem to not influence the final result.
d) Although a more detailed study of the inlet conditions needs to be done, the current results seem to show that if the detectors are far away from the building domain, the inlet conditions have a more prominent effect at locations higher up (line L9) as opposed to locations nearer the source height (lines L7 and L8). For detectors far away from the building area but near the ground level, all three inlet conditions give very similar results (line L10), especially for detectors “north” of the source.

4. Effects of tall buildings on pollution dispersion

Having demonstrated the ability of the LES model to predict dispersion in the vicinity of building complexes, we move to the main purpose of the present research, namely to illustrate the

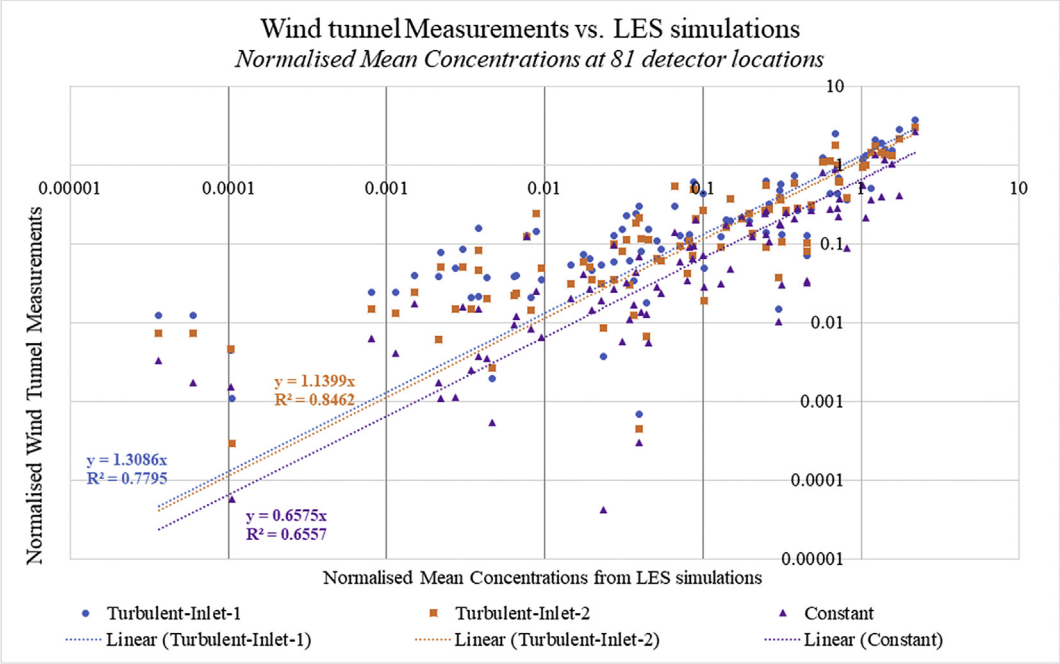

Fig. 3. A scatter plot showing the comparison of the LES simulation results vs. the wind tunnel measurements.

effects that nearby tall buildings have on the distribution of concentration resulting from emissions from the Building A stack. To recap, the source of pollution is centred at $x = y = 0$ m, $z = 0.1508$ m above the centre of a "low-rise" building (0.1428 m high at model scale, corresponding to 28.56 m for a scale factor of 1:200). The configuration examined in the validation study defines the base case, Case 1. Two additional scenarios (Case 2 and Case 3) were considered in which the heights of all buildings (Table 1) were increased, except for the building where the source was located (Building A, the Garden building). The concentration fields are shown and discussed in the main paper, whilst additional supporting information, particularly information associated with the air flows (velocity fields) are included in the supporting document (S4 to S11).

4.1. Concentration isosurfaces

One of the most effective visual representations of pollution dispersion in a three-dimensional space is the iso-surface representation. Thus, the simulations results for the three cases were plotted as concentration iso-surfaces (non-normalised concentration values) as shown in Fig. 5, showing clearly the contrasts between the three cases. Fig. 5 (a) shows pollution dispersion for the base case, Case 1, in which concentrations are persistently high downstream of the building complex. Fig. 5(b) and (c) (Cases 2 and 3) show 'shorter' plumes downwind of the site but more widely dispersed pollution amongst the site buildings. The latter feature is most pronounced in Case 3, where the height of Building F has been further increased from Case 2. The taller buildings create larger downwind recirculation regions and greater flow deflections than the base case and the associated flow fields drive the changes in dispersion behaviour. Further detail can be derived from the two-dimensional cross-sections through the concentration fields shown in Figs. 6–8 that are discussed in Sections 4.2–4.4. That these do not necessarily cut through regions of greatest concentrations – or that the location of the planes relative to the plumes in each case may be different – needs to be borne in mind when interpreting these figures.

4.2. Horizontal (x-y) plane at height $z = 0.1508$ m (source height)

Fig. 6 shows the tracer dispersion results for all three cases in the horizontal plane at source height. Dispersion patterns are clearly a direct consequence of the flow patterns associated with each case, as shown in the supporting document (S4 and S5) - which also show the very detailed adaptive mesh generated and required to capture accurately the turbulent flow and dispersion patterns at high spatial resolution. It is clear from S4 and S5 that the cases with taller buildings (Case 2 and Case 3) have different dominant flows and re-circulation patterns when compared to the base case (Case 1), influencing the subsequent nature of dispersion. The adaptive mesh for the concentration field is shown in the supporting document (S6) – following the adaptivity metrics based on concentration and velocity values.

The results clearly show that:

- When the velocity fields are weaker, the concentrations of pollution are higher (sometimes an increase an increase of 100% around building A for example). Dispersion patterns within the building area differs between Cases 2 and 3, due to the much taller building F in Case 3. Stronger velocity fields lead to lower concentrations (by nearly 75% decrease in some locations e.g. between buildings D and E) – as it is evident in Case 3. Also, a stronger velocity field between buildings A and C and buildings F and E lead to no polluted regions between these buildings.
- The extended downstream dispersion pattern shown in Case 1 no longer exists when the heights of the buildings surrounding the source building are increased, as in Cases 2 and 3. Downwind concentrations are lower (by as high as 90% decrease) for Cases 2 and 3.
- The presence of the taller F-building (Case 3) generates a stronger circulation pattern between buildings A, C and D, and thus pollution concentrations in front of building C are now virtually non-existent with pollution concentrations higher on

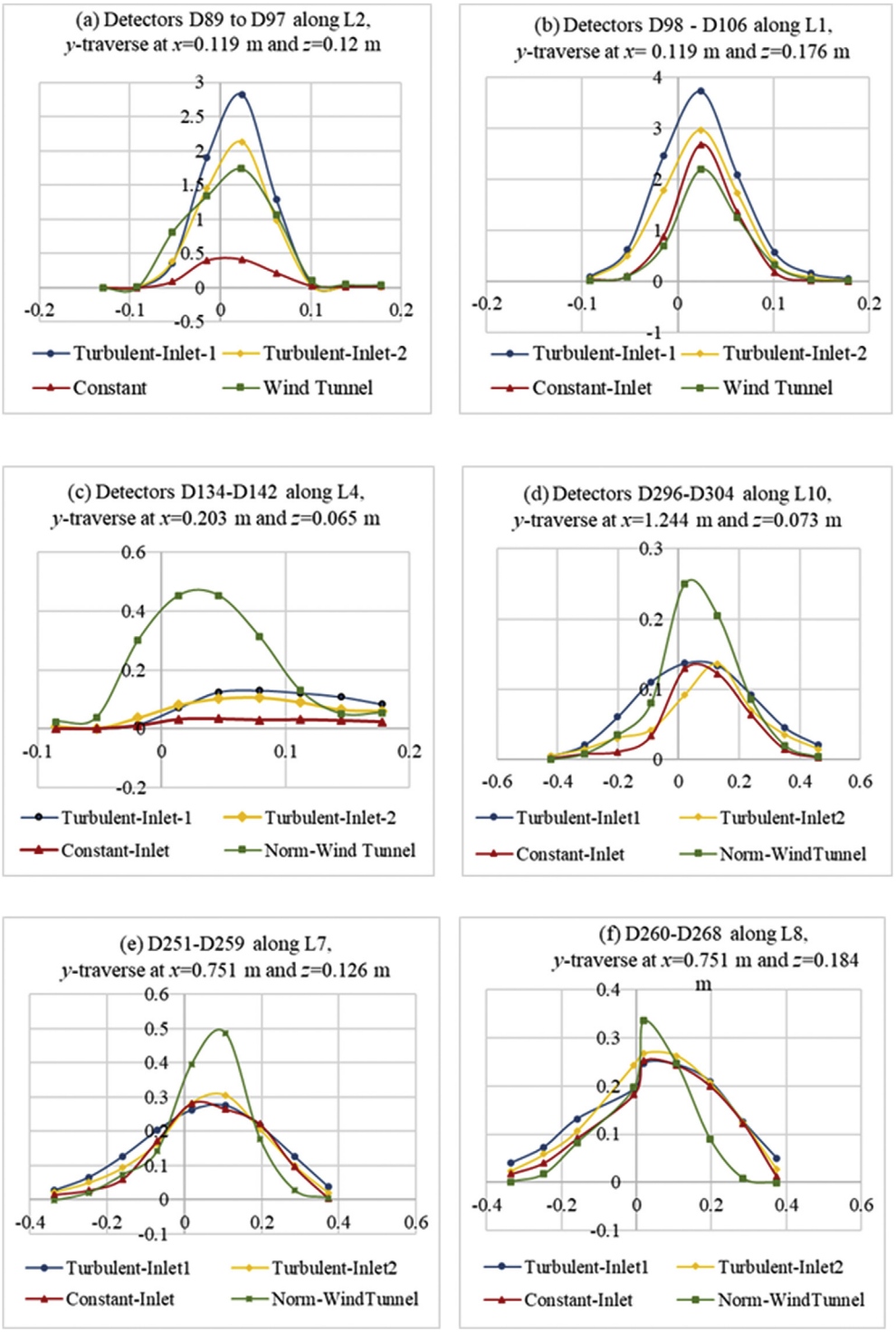

Fig. 4. Six plots (a) to (f) showing the comparison of *normalised mean concentrations* between wind tunnel data and FLUIDITY simulations for several detectors along different *lateral traverses (x-lines)*. Llocation of the detectors is indicated in each plot. *Note: Horizontal Axis:* Distance in metres; *Vertical axis:* Normalised mean concentrations.

top of the building A, and around building D. The pollution around building A also finds an "escape" route through the gap between buildings D and E, where concentrations are decreased by 300%; to the contrary, however, concentrations around building C (downwind side) has increased by nearly 300%.

Thus, comparing the three cases in the (*x*-*y*) horizontal plane, at source height, it is clear when the heights of the surrounding buildings (Cases 2 and 3) are increased relative to the source building, greater concentrations are experienced between the buildings (A, C, D), with buildings C and D being particularly affected.

4.3. Vertical (x-z) plane at y = 0.0 m

The effect of the tall buildings on the pollution concentrations in

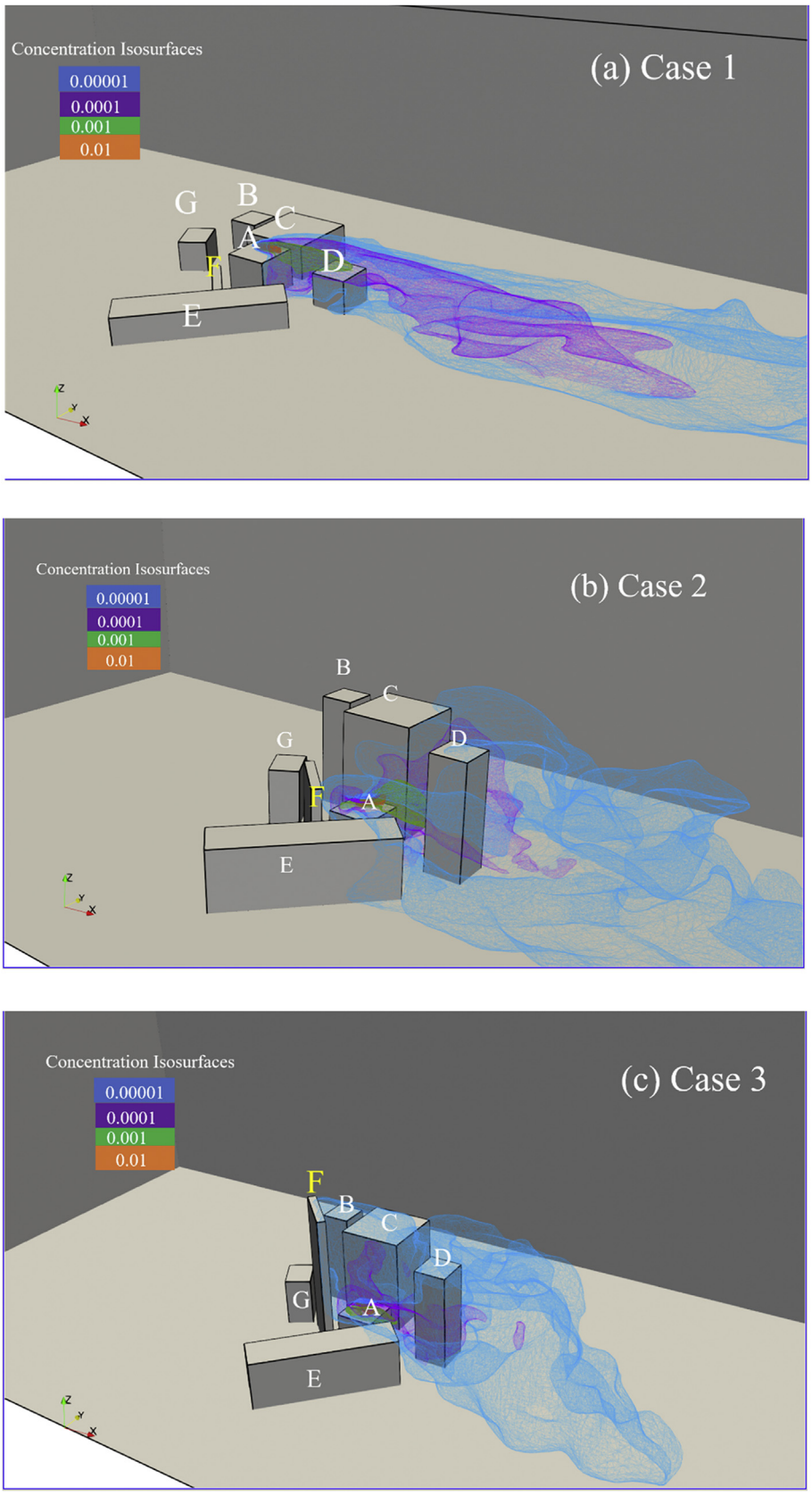

Fig. 5. Concentration iso-surfaces for Cases 1, 2 and 3, showing how the presence of tall buildings affects pollution dispersion within a local neighbourhood. The effect of the taller buildings is clearly illustrated in the simulations – with the higher pollution concentrations (e.g. isosurface 0.0001 - purple colour) remaining within the building complex for Cases 2 and 3, contrary to Case 1 where it spreads downwind the building area.

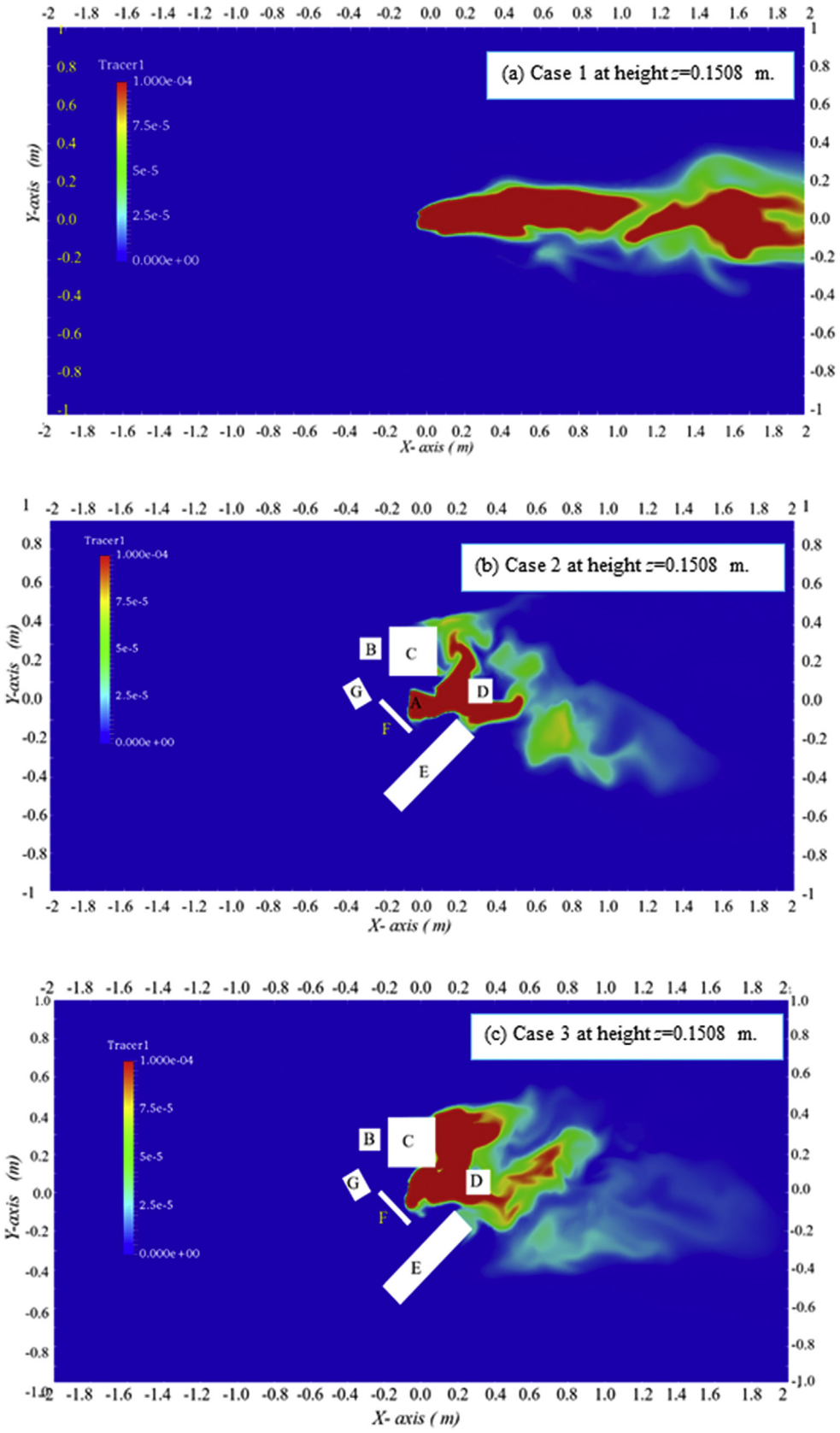

Fig. 6. Concentration maps in the horizontal plane (*x*-*y*) view at *source height* $z = 0.1508$ m of Tracer dispersion for the three cases: (a) Case 1; (b) Case 2; (c) Case 3. The effect of the taller buildings is clearly seen.

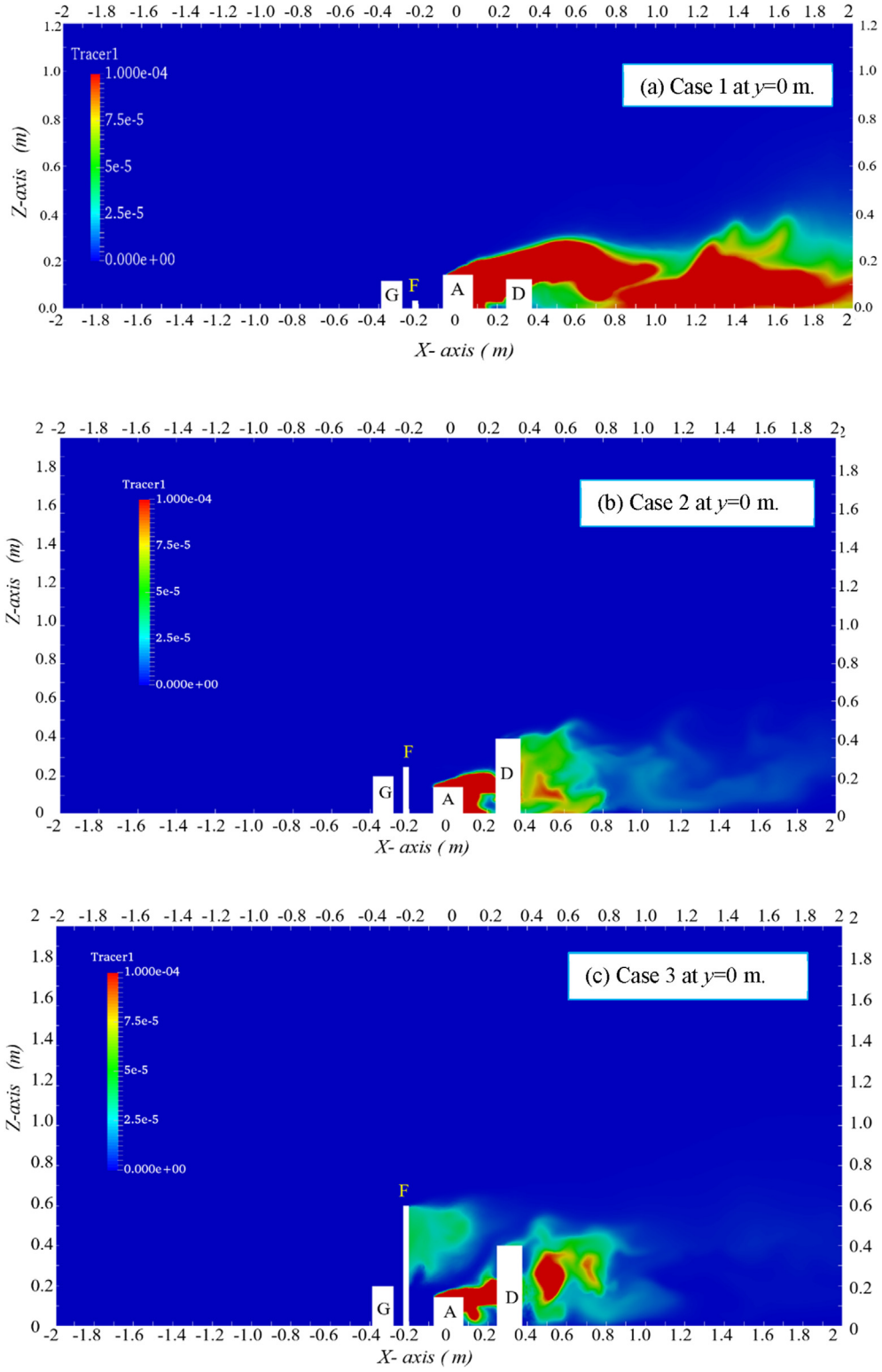

Fig. 7. Concentration maps in vertical plane (x-z) view through the centre of the domain ($y = 0$), for the three cases: (a) Case 1; (b) Case 2; (c) Case 3. The effect of the tall buildings is clearly seen.

the (x-z) plane are shown in Fig. 7. The corresponding velocity fields generated for the three cases are shown in the supporting document (S7 and S8), with the distinctive changes due to the presence the tall buildings, especially the presence of the tall building F in Case 3 clearly seen. The increased height of building F in Case 3 has generated a low-velocity region immediately downstream of building F, but also a circulation pattern in the central area and above building A (the source building), with a region of strong flow moving towards the right of the domain above building A, and towards building D.

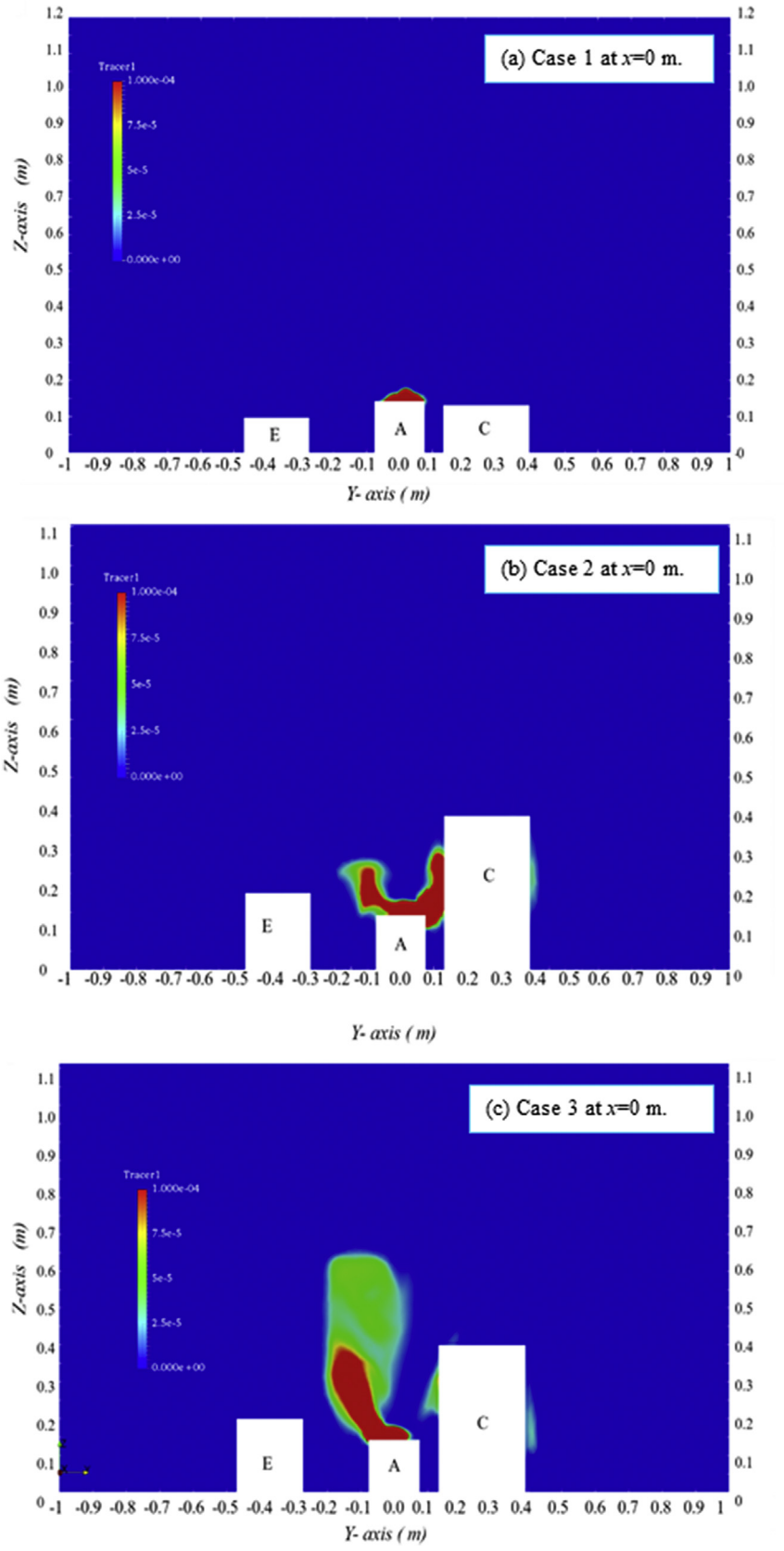

Fig. 8. Concentration maps in vertical plane (y-z) at the centre of the domain ($x = 0.0$ m), for the three cases: (a) Case 1; (b) Case 2; (c) Case 3.

These variations in the velocity fields (seen in the supplementary document S7 and S8) have a major effect on the tracer dispersion as seen in Fig. 7. For the base case (Case 1), the pollution flows above the building-area at a persistent height of ~0.12 m for a distance nearly twice the distance of building D from the source (hence for ~0.8 m), after which pollution concentrates at lower levels till the end of the computational domain. For Cases 2 and 3, however, pollution concentrations are higher just downstream of building D, whilst for distances beyond 0.8 m concentrations are much lower (as opposed to Case1).

It is interesting to notice that although there are high concentration levels above and around the building A, no pollution finds its way to the left of building A (i.e. in regions between buildings A and F or A and G), despite the weak flow fields in these regions. The simulations show clearly that the tracer dispersion patterns observed in the base case (Case 1) are quite different to those observed for Cases 2 and 3. Several features are particularly notice worthy:

- The *pollution-free* regions (regions between A and E and between A and F) observed in Case 1 are not sustained, when the heights of the buildings surrounding building A are increased, as can be seen particularly in Case 3. Pollution appears at higher levels of building F on its downwind side, which was previously *pollution free*; the lower levels remain pollution free. It would be interesting to determine the "optimal" height of building F, which would reduce concentration levels at all heights.
- Concentrations of pollution downstream of building D are higher for Case 3 than in Case 2 showing how the height of building F plays a major role in determining the downstream pollution concentrations.
- All Cases show high concentrations levels between buildings A and D at heights below their roof height. However, in each case, there is a slight variation in the area most polluted between the two buildings, with concentration increases of 100%; the locations where these increases occur very much depends on the heights of the buildings D and F, emphasising the role they play in determining as dispersion conditions.

These results have clear implications for the urban/city design point of view; the comparisons clearly show the degree to which the increased building heights around the source building affect the distribution of pollution, with Case 3 being the worst case.

4.4. Vertical (*y*-*z*) plane at $x = 0.0$ m

The (*y*-*z*) plane is normal to the incoming velocity vector (*x*-component only) and viewing results in this cross-section allows us to see the results between buildings E, A and C only, due to the configuration of the buildings; building F, whose height changes dramatically between Cases 1, 2 and 3, is not seen in this plane; however, its effect is observed in both the velocity fields and pollution patterns, particularly for Cases 2 and 3.

The concentration results for the three cases are shown in Fig. 8, whilst the associated velocity fields are included in the supporting document (S9 and S10). Additional information showing the detailed adaptive meshes for the concentration fields is also given in the supplementary document (S11). The velocity field changes significantly as the building heights are increased (Cases 2 and 3), especially around building F for Case 3 (S9 and S10). The dispersion results shown in Fig. 8 reflect the velocity distributions for all three cases. The main features of the concentration fields observed in this (*y*-*z*) plane are:

The main features of the concentration fields observed in this (*y*-*z*) plane are:

- Limited vertical dispersion above building A in the base case (Case 1).
- Greatly enhanced vertical pollution concentrations, with pollution spreading upwards in regions which were previously pollution free – in regions vertically between buildings E and A, in Cases 2 and 3.
- Pollution free zones on the left of building A in Case1 became contaminated with pollution in Cases 2 and 3, especially when the height of building F was highest (Case 3). An interesting plume appears on the left of building A for Case 3, in the region between building A and E. High concentrations are seen rising well above the height of building A due to the interesting low velocity field within this region (S9 and S10).
- Some pollution levels are detected around building C, for both Cases 2 and 3, in regions which were pollution-free in Case 1.

These results, especially for Cases 2 and 3 emphasise the importance of the height of buildings within very localised regions around them, as they show increased pollution levels in such regions which were previously pollution free – occurring in different locations within the domain, depending on the height of the surrounding buildings (e.g. contrast Cases 2 and 3), and thus highlighting the potential importance of detailed CFD studies in guiding design on new high-rise developments.

5. Conclusions

We have implemented a novel, unstructured and adaptive-mesh LES flow solver with an anisotropic, eddy-viscosity model that is linked to the anisotropic adaptive mesh. The method captured successfully both the complex air flows and dispersion patterns in a small building complex at high spatial resolution. The validation study using wind tunnel dispersion measurements for a specific seven-building configuration showed satisfactory correlations between observed and predicted normalised, mean concentrations over and downwind from the site, the source being at roof level on a building in the centre of the complex. Two further computational studies were then set-up to assess the effect of increased building heights surrounding the source. The results clearly showed how increasing this led to a worsening of pollution levels within the site, with a much wider spread of pollutants into regions formerly pollution-free. However, concentration levels downwind from the site were generally reduced.

These results highlighted the importance of detailed air flow and dispersion modelling within an urban environment prior to any new building developments that would involve high/tall buildings. The changing cityscapes due to the continuous rise of such multi-storey buildings and the possibility of emission sources within the urban environment (due to the presence of CHPs) necessitates such detailed computational and physical modelling to optimise the design of new buildings and control the exposure of the urban population to harmful air pollutants. As it is seen from the results, simply changing the height of a single building can have negative effects on pollution levels on-site. Thus, assessing the effect of building designs/heights through complex modelling (CFD or wind tunnel) may become a necessary step in designing a sustainable and healthy urban environment.

This was an illustrative rather than a generic study, to be followed by more systematic research aimed at generalising conclusions and understanding processes sufficiently to provide broad design guidance.

Acknowledgements

We would like to thank the reviewers for their very constructive

comments on this research. This work was initiated by a Master programme within the Environmental Policy Centre at Imperial College London, followed by further computational modelling work using the Imperial College FLUIDITY software within the School of Engineering at LSBU. The wind tunnel measurements were carried out at the Enflo wind tunnel at the University of Surrey. This work currently forms part of the EPSRC MAGIC project No: P58094. C. Pain acknowledges the support from the European Union Seventh Framework Programme (FP7/200 72013) under grant agreement NO. 603663 for the research project PEARL (Preparing for Extreme and Rare events in coastal regions).

Appendix A. Supplementary data

Supplementary data related to this article can be found at https://doi.org/10.1016/j.envpol.2017.10.041.

References

Aristodemou, et al., 2016. Simulating turbulent air flows in central London and studying effect of tall buildings. In: HARMO17 Conference. Budapest, Hungary, May 2016. http://www.harmo.org/Conferences/Proceedings/_Budapest/publishedSections/H17-160.pdf.

Aristodemou, E., Bentham, T., Pain, C., Robins, A., 2009. A comparison of mesh-adaptive LES with wind tunnel data for flow past buildings: mean flows and velocity fluctuations. Atmos. Environ. 43, 6238–6253.

Baik, J.J., Kim, J.J., 2002. On the escape of pollutants from urban street canyons. Atmos. Environ. 36, 527–536.

Baker, J., Walker, H.L., Cai, X., 2004. A study of the dispersion and transport of reactive pollutants in and above street canyons – a large eddy simulation. Atmos. Environ. 38, 6883–6892.

Belcher, S.E., Coceal, O., Goulart, E.V., Rudd, A.C., Robins, A.G., 2015. Processes controlling atmospheric dispersion through city centres. J. Fluid Mech. 763, 51–81.

Benson, R.A., McRae, D.S., 1991. A solution adaptive mesh algorithm for dynamic/static refinement of two and three-dimensional grids. In: Proceedings of the 3rd International Conference on Numerical Grid Generation in Computational Field Simulations. Barcelona, Spain, 1991.

Bentham, T., 2004: PhD thesis, Imperial College, London.

Carpentieri, M., Robins, A.G., 2015. Influence of urban morphology on air flow over building arrays. J. Wind Eng. Industrial Aerodynamics 145, 61–74.

Caton, F., Britter, R.E., Dalziel, S., 2003. Dispersion mechanisms in a street canyon. Atmos. Environ. 37, 693–702.

Coceal, O., Dobre, A., Thomas, T., Belcher, S., 2007. J. Fluid Mech. 589, 375–409.

Coirier, W., Fricker, D., Furmanczyk, M., Kim, S., 2005. A computational fluid dynamics approach for urban area transport and dispersion modeling. Environ. Fluid Mech. 5, 443–479.

Constantinescu, E., Sandu, A., Carmichael, G., 2008. Modelling atmospheric chemistry and transport with dynamic adaptive resolution. Comput. Geosci. 12, 133–151.

Cui, D.J., Mak, C.M., Kwok, K.C.S., Ai, Z.T., 2016. CFD simulation of the effect of an upstream building on the inter-unit dispersion in a multi-story building in two wind directions. J. Wind. Eng. Ind. Aerodyn. 150, 31–41.

Di Sabatino, S., Buccolieri, R.B., Pulvirenti, B., Britter, R.E., 2008. Flow and pollutant dispersion in street canyons using FLUENT and ADMS-Urban. Environ. Model Assess. 13, 369–381.

Fluidity Manual, 2016. AMCG group, Imperial College London. https://github.com/FluidityProject.

Ghorai, S., Tomlin, A., Berzins, M., 2000. Resolution of pollutant concentrations in the boundary layer using a fully 3d adaptive gridding technique. Atmos. Environ. 34, 2851–2863.

Gorman, G., Pain, C., Oliveira, C., Umpleby, A., Goddard, A., 2003. In: International Conference on Supercomputing in Nuclear Applications.

Gromke, C., Blocken, B., 2015. Influence of avenue-trees on air quality at the urban neighbourhood scale: Part I: quality assurance studies and turbulent Schmidt number analysis for RANS CFD simulations. Environ. Pollut. 196, 214–223.

Heist, et al., 2009. The effect of a tall tower on flow and dispersion through a model urban neighbourhood. Part1. Flow characteristics. J. Environ. Monit. 11, 2163–2170.

Hong, B., Lin, B., 2015. Numerical Studies of the outdoor wind environment and thermal comfort at pedestrian level in housing blocks with different building layout patterns and trees arrangement. Renew. Energy 73, 18–27.

Janhall, S., 2015. Review of urban vegetation and particle air pollution – deposition and dispersion. Atmos. Environ. 105, 130–137.

Jarrin, N., Benhamadouche, S., Laurence, D., Prosser, R., 2006. A synthetic eddy-method for generating inflow conditions for large-eddy simulations. Int. J. Heat Fluid Flow 27, 585–593, 2006.

Kim, J.J., Baik, J.J., 2003. Effects of inflow turbulence intensity on how and pollutant dispersion in an urban street canyon. J. Wind Eng. Industrial Aerodynamics 91, 309–329.

Luo, K., Yu, H., Dai, Z., Fang, M., Fan, J., 2016. CFD simulations of flow and dust dispersion in a realistic urban area. Eng. Appl. Comput. Fluid Mech. 10 (1), 228–242. https://doi.org/10.1080/19942060.2016.1150205.

Milliez, M., Carissimo, B., 2007. Numerical simulations of pollutant dispersion in an idealized urban area for different meteorological conditions. Bound. Layer. Meteorol. 122, 321–342.

Odman, M.T., Mathur, R., Alapaty, K., Srivastava, R.K., McRae, D.S., Yamartino, R.J., 1997. Nested and adaptive grids for multiscale air quality modeling. In: Delic, G., Wheeler, M.F. (Eds.), Next Generation Environmental Models and Computational Methods. SIAM, Philadelphia, pp. 59–68.

Pain, C., Umpleby, A., de Oliveira, C., Goddard, A., 2001. Comput. Methods Appl. Mech. Eng. 190, 3771–3796.

Pavlidis (2010) Ph.D. Thesis, Imperial College London.

Piomelli, 1999. Large eddy simulations: achievements and challenges. Prof. Aerosp. Sci. 35 (4), 335–362.

Porte-Agel, F., 2004. A scale-dependent dynamic model for scalar transport in large-eddy simulations of the atmospheric boundary layer. Boundary-Layer Meteorol. 112, 81–105.

Pope, S., 2000. Turbulent Flows. Cambridge University Press.

Robins, 2016. Personal Communication.

Sagaut, 1998. Large Eddy Simulation for Incompressible Flows. Springer.

Smagorinsky, J., 1963. General circulation experiments with the primitive equations. Mon. Weather Rev. 91, 99–164. ftp://ftp.library.noaa.gov/docs.lib/htdocs/rescue/mwr/091/mwr-091-03-0099.pdf.

Solazzo, E., Britter, R., 2007. Transfer processes in a simulated urban street canyon. Boundary-Layer Meteorol. 124, 43–60.

Střižík, M., Zelinger, Z., Nevrlý, V., et al., 2014. CFD modelling for atmospheric pollutants/aerosols studies within the complex terrains of urban areas and industrial sites. Int. J. Environ. Pollut. 54 (1), 73–90.

Srivastava, R.K., McRae, D.S., Odman, M.T., 2000. An adaptive grid algorithm for air quality modeling. J. Comput. Phys. 165, 437–472.

Srivastava, R., McRae, D., Odman, M., 2001a. Simulation of a reacting pollutant puff using an adaptive grid algorithm. J. Geophys. Res. 106, 24245–24257.

Srivastava, R., McRae, D., Odman, M., 2001b. Simulation of dispersion of a power plant plume using an adaptive grid algorithm. Atmos. Environ. 35, 4801–4818.

Tomlin, A.S., Berzins, M., Ware, J., Smith, J., Pilling, M.J., 1997. On the use of adaptive gridding methods for modelling chemical transport from multi-scale sources. Atmos. Environ. 31, 2945–2959.

Tong, Z., Chen, Y., Malkawi, A., Adamkiewicz, G., Spengler, J.D., 2016. Quantifying the impact of traffic-related air pollution on the indoor air quality of a naturally ventilated building. Environ. Int. 89-90, 138–146.

Toparlar, Y., Blocken, B., Vos, P., Van Heijst, G., Janssen, W., Van Hooff, T., Montazeri, H., Timmermans, H., 2015. CFD simulation and validation of urban microclimate: a case study for Bergpolder Zuid, Rotterdam. Build. Environ. 83, 79–90.

Walton, A., Cheng, A.Y.S., 2002. Large Eddy simulation of pollution dispersion in an urban street canyon: Part II: idealised canyon simulation. Atmos. Environ. 36 (22), 3615–3627.

Wissink, A., Chand, K., Kosovic, B., Chan, S., Berger, M., Chow, F.K., 2005. Adaptive Urban Dispersion Integrated Model. 86th American Meteorological Society Annual Meeting. Atlanta, GA, USA. UCRL-PROC-216813.

Xie, S.D., Zhang, Y.H., Li, Q., Tang, X.Y., 2003. Spatial distribution of traffic-related pollutant concentrations in street canyons. Atmos. Environ. 37 (23), 3213–3224.

Yu, et al., 2017. Air pollutant dispersion around high-rise buildings under different angles of wind incidence. J. Wind Eng. Industrial Aerodynamics 167, 51–61.

Zhang, N., Du, Y., Miao, S., 2016. A microscale model for air pollution dispersion simulation in urban areas: presentation of the model and performance over a single building. Adv. Atmos. Sci. 33, 184–192.

Zhiyin, Y., 2015. Large-eddy simulation: past, present and the future. Chin. J. Aeronaut. 28 (1), 11–24.

Zhou, Y., Hanna, S., 2007. Along-wind dispersion of puffs released in a built-up urban area. Boundary-Layer Meteorol. 125, 469–486.